Sixth International Symposium on Turbulence and Shear Flow Phenomena
Seoul, Korea, 22-24 June 2009

DNS OF OSCILLATING RIBLETS FOR TURBULENT DRAG REDUCTION

Felix Kramer, Frank Thiele, Erik Wassen
Institut für Strömungsmechanik und Technische Akustik,
Technische Universität Berlin
Straße des 17. Juni 135, Sekr. MB1, 10623 Berlin, Germany
felix.kramer@cfd.tu-berlin.de

ABSTRACT

Blade-shaped riblets are tilted sinusoidally at specific frequencies to reduce turbulent friction drag. Within this investigation, the overall drag reduction of stationary riblets could be improved by the oscillation from 8.6% to 11.1%. Two examplary cases are presented, one showing an increase in drag reduction and one with only minor changes compared to stationary riblets. Detailed analysis of data from direct numerical simulations reveals that the additional drag reduction is mostly related to a smaller contribution from the riblet tips which is caused by a secondary motion of low-speed fluid. The effect is accompanied by a reduction of turbulent activity within the main flow.

INTRODUCTION

Different riblet configurations have been investigated in the past (Walsh, 1990; Bechert, 1989) and have achieved friction drag reduction of up to 10% for blade-shaped riblets. It is a *passive* technique and has already been applied in commercial products. Another well-known method of drag reduction is a laterally oscillating smooth wall (Jung, 1992; Laadhari, 1994; Baron, 1996; Trujillo, 1997; Miyake, 1997; Choi K.S., 1998, 2001; Karniadakis, 2003) which is *actively* driven and thus energy consuming but achieves a drag reduction up to 45% (Choi K.S., 1998). The induced lateral motion hampers the streamwise vortices and reduces the streak and burst activity in the boundary layer (Miyake, 1997; Karniadakis, 2003).

This investigation combines the stationary riblets with the very effective oscillating wall by tilting riblets sinusoidally. Compared to the smooth oscillating wall the blade-shaped riblets induce a similar lateral momentum at a certain distance from the wall (Wassen, 2008). The lateral momentum is necessary to affect the coherent structures in the buffer layer.

NUMERICAL SETUP

The direct numerical simulations are performed in a fully turbulent channel at $Re_\tau = 360$, based on the shear velocity u_τ and the channel height H. The length of the channel in streamwise direction is $3H$, and the width in spanwise direction is $1.5H$. Therefore, the channel is not completely de-correlated (Kim, 1987) but is still significantly larger than the "minimal flow unit" (Jimenez, 1991) which is necessary to simulate near wall structures of turbulent flow. The channel's top wall is smooth as depicted in figure 1 and provides a direct reference to the bottom wall which carries the blade-shaped riblet surface consisting of 32 segments in spanwise direction. All walls are impermeable and have no slip. The remaining sides perpendicular to the streamwise and the spanwise direction are periodic boundaries. The newtonian and incompressible fluid is driven by a constant streamwise pressure gradient. Depending on time and investigated surface, the resulting Reynolds number based on the bulk velocity u_b varies between 5700 and 5900. The flow solver uses a finite-volume discretization of second order accuracy in time and space on a structured grid of 11 million cells. The time-averaged data used throughout this paper covers an interval of a least 320 convective units based on the time-averaged bulk-velocity and the channel height.

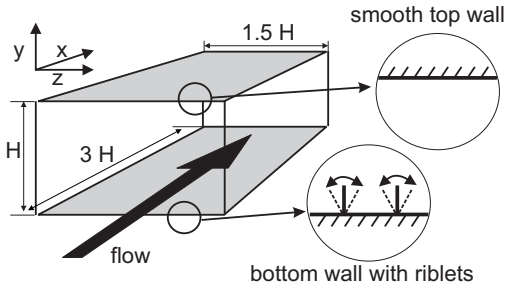

Figure 1: Computational domain.

The sinusoidal oscillation of the tilting riblets has a maximum angle of 30° while keeping the riblets stiff and synchronized. Each riblet's height, $h^+ = h\frac{u_\tau}{\nu}$, is 8.96 wall units, and the spacing between two adjacent riblets, $s^+ = s\frac{u_\tau}{\nu}$, is 16.875 wall units where ν denotes the kinematic viscosity. The geometrical setup fits well with the optimal stationary riblets according to Bechert (1997).

This paper compares the results from DNS of two different periods of oscillation $T^+ = T_{osc}\frac{u_\tau^2}{\nu}$ applied to the described geometry. The first case (A) oscillates at $T^+ = 35$,

Table 1: Basic parameters and results.

		case A	case B
period of oscillation	T^+	35	100
riblet height in wall units	h^+	8.96	8.96
riblet spacing in wall units	s^+	16.875	16.875
lateral top speed of riblet tips	w^+_{tip}	0.85	0.29
average Reynolds number	$\overline{Re_{u_b}}$	5826	5770
drag reduction		11.1%	8.4%

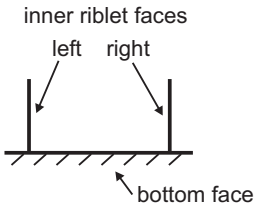

Figure 2: Notation of riblet faces.

reaching a top speed of $w^+_{\text{tip}} = 0.85$ at the riblet tips. The second case (B) has a slower oscillation of $T^+ = 100$ which is considered to be a very effective period of the well-known laterally oscillating wall.

DRAG AND WALL SHEAR STRESS

Integrating the wall shear stress of all surfaces allows to calculate the friction drag difference between the smooth top wall and the bottom wall with the oscillating riblets. Increasing this difference is the main aim of this study. The stationary reference case without oscillation achieved a drag reduction of 8.6% (Wassen, 2008). The slower oscillation of case B achieves 8.4% whereas the faster oscillation of case A shows a drag reduction of 11.1%.

A first order approach to analyze this gap between both cases is to locate the drag gain in space and time. Therefore, the spatial distribution of the wall shear stress is plotted in figure 3. The underlying data is obtained from the phase-averaged flow at a phase angle of 0° which corresponds to vertical, non tilted riblets moving to the right. The wall shear stress is normalized by the smooth top wall's shear stress and plotted for three different representative faces of homogeneously averaged riblet segments. The bottom face in the center of figure 3 shows only small differences in the ascending part. The asymmetric behavior is due the phase angle at which the riblets are moving to the right. However, the inner *right* riblet face reveals a more pronounced shift to the advantage of case A which grows steadily with greater y^+ and reaches its maximum at the riblet tips. For the whole inner right riblet face, case A produces less drag than case B. The inner *left* riblet face behaves differently. Starting at $y^+ = 0$, case A is slightly below case B at first. But above $y^+ = 6$, case A outperforms case B, resulting in a smaller shear stress at the riblet tip comparable to the one of the inner right riblet face. The asymmetry of both riblet faces is once again related to the actual phase angle. Half a period later, the distribution is interchanged. Looking at the whole distribution, the main advantage of case A is located at the riblet tips whereas the bottom face seems to have very small impact.

The development over time in terms of phase angle is plotted in figure 5. The drag contribution of each face is

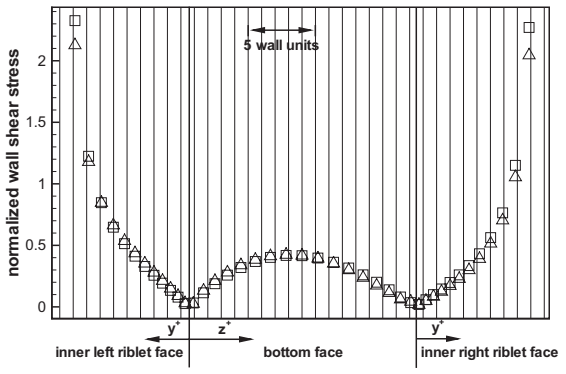

Figure 3: Phase-averaged wall shear stress of the three representative lower wall faces at a phase angle of 0° and normalized by the wall shear stress of the respective upper wall. △ $T^+ = 35$ (case A), □ $T^+ = 100$ (case B).

plotted separately for all phase angles. The values are normalized by the drag of the smooth top wall, i.e. a value of 1.0 means that the drag of the specific face equals the drag on the top wall. In addition, the time-averaged values are summarized in table 2. The drag contribution of the bottom face in figure 5(a) is slightly elevated and phase-shifted for case A. Comparing to table 2, the integrated difference is 0.01 fraction points to the disadvantage of case A, supporting the earlier results from the spatial distribution. The right riblet face of case A in figure 5(b) shows a better performance than case B for the first half of the period until being back in upright position. During the second half period the inner right faces show only marginal differences.

When regarding the sum of all faces in figure 5(c), the maximum drag improvement of case A compared to case B is achieved in the upright positions at $t^* = 0$ and $t^* = 0.5$. But the largest overall drag reduction compared to the top wall is obtained when the riblets are entirely tilted at $t^* = 0.25$ and $t^* = 0.75$. At this phase angle no difference can be observed between the two cases.

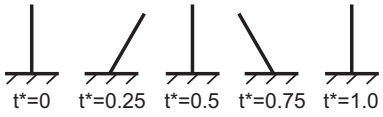

Figure 4: Sketch of riblets at different phase angles.

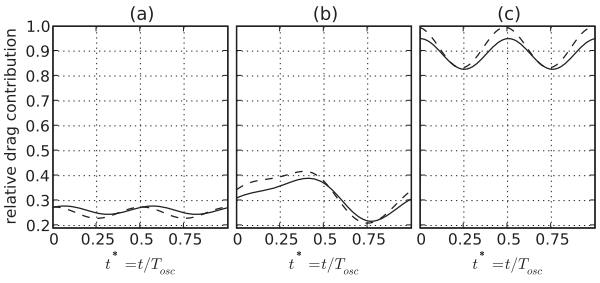

Figure 5: Phase-wise drag for the different contributing surfaces normalized the top wall's drag. (a) bottom face, (b) inner side of right riblet, (c) sum of all bottom faces. —— $T^+ = 35$ (case A), – – – $T^+ = 100$ (case B).

Table 2: Time-averaged drag contribution of different faces as in figure 5 with respect to smooth wall drag.

	case A	case B
bottom face	0.262	0.252
single riblet face	0.314	0.331
first half period	0.357	0.392
second half period	0.270	0.271
sum of riblet faces	0.627	0.662
sum of all faces	0.889	0.914

SECONDARY MOTION

In contrast to a smooth wall, the geometrical shape of riblets induces secondary motions that can be found in the temporal averaged wall-normal (v) and spanwise (w) velocity components. Wall-normal motion increases the transport of momentum to and away from the wall and is often responsible for drag increase. For stationary riblets, this motion is very weak compared to the oscillating riblets. Figures 6 and 7 show contours of the wall-normal velocity component normalized by the shear velocity u_τ at a phase angle of 0°. Two lobes of upward moving fluid can be observed at the riblet faces. This upward motion is complemented by a downward flow between the riblets. These motions are considerably strong compared to the streamwise velocity component. The largest value of the downward motion from figure 6 is 4% of the averaged u component. For the slower oscillation of case B in figure 7 it is only 1%. Interestingly, the stronger downward motion of case A leads only to a slightly higher drag on the bottom face. At the same time it induces a stronger upward motion. The peak of the upward motion of case A on the left of the right riblet tip reaches up to 19% and transports slow fluid upwards along the right riblet. Case B is once again four times weaker and achieves 5%. The location and the time of this strong difference in upward motion corresponds exactly to the time and location of the largest drag difference from figures 5(b) and 3. This strongly indicates that the transport of slow fluid from the riblet groove "protects" the riblet tips and reduces the streamwise wall shear stress.

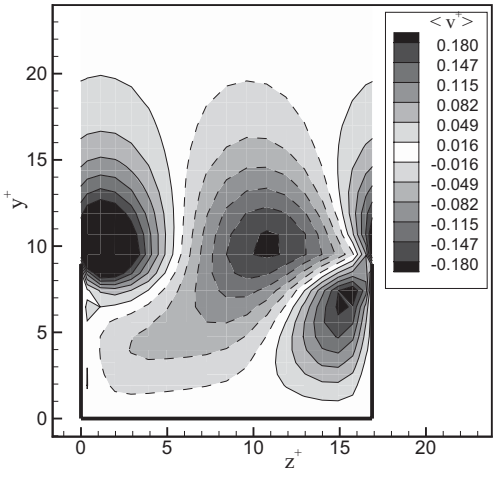

Figure 6: Contours of phase-averaged wall-normal velocity for case $T^+ = 35$ at a phase angle of 0°. Dashed lines indicate negative values.

TURBULENT ACTIVITY

In addition to the differences in wall shear stress between the two cases there are also differences in the flow field above the riblets. Figure 8 shows the contours of the streamwise velocity fluctuation at a phase angle of 0°. Compared to the smooth wall, both cases damp the fluctuation and shift the maximum upwards. Consistent to the above observations, case A reduces the streamwise velocity fluctuation above the riblets better than case B. The contour lines above $y^+ = 15$ demonstrate nearly no spanwise variation although the riblets are reaching up to $y^+ \approx 9$.

To estimate the influence on coherent structures and vortices, the vortex indicator Q is used. Q is the positive second invariant of the velocity gradient ∇u:

$$Q = \frac{1}{2}\left(||\Omega||^2 - ||S||^2\right) \tag{1}$$

Here, Q stands for the balance between the local vorticity magnitude $||\Omega||$ and the shear strain rate $||S||$. Positive values of scalar Q mean stronger vorticity than strain and indicate an overweight of vortical flow conditions. For the present cases, the phase-averaged Q is approximately -0.1 and has a standard deviation of 0.1 above the riblets. However, when looking for effects on vortices, it is more appropriate to average only positive values by using the Heaviside function $H(\cdot)$ as in equation 2:

$$Q_H := H(Q) \tag{2}$$

Figure 9 shows the contour lines of the phase-averaged Q_H for both cases and a smooth reference wall. The extreme values at the riblet tips have mainly two reasons. Since the calculation of Q is based on gradients of the velocity components, the infinitely sharp riblets produce singularities. But the effect is limited to the riblet tips and values further away are not influenced by these singularities. The second reason is that the riblet tips generate a weak, persistent vortex at the observed phase angle. The vortex turns up stronlgy because the phase-averaging is exactly synchronized to this phase angle and consequently to the vortex.

The maximum of the smooth wall's Q_H at $y^+ = 25$ is much larger than those of the two oscillating cases. As already observed in the streamwise velocity fluctuations, the contour lines above a certain height demonstrate nearly no

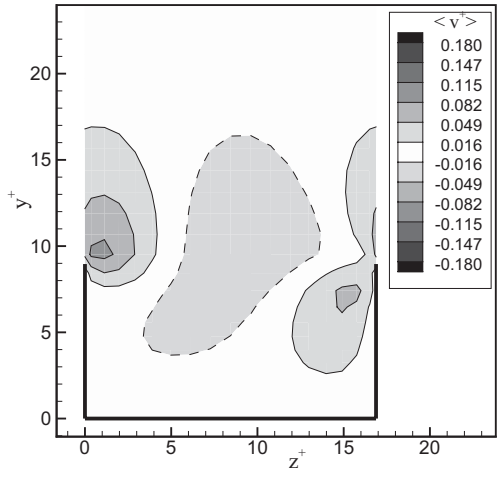

Figure 7: Contours of phase-averaged wall-normal velocity for case $T^+ = 100$ at a phase angle of 0°. Dashed lines indicate negative values.

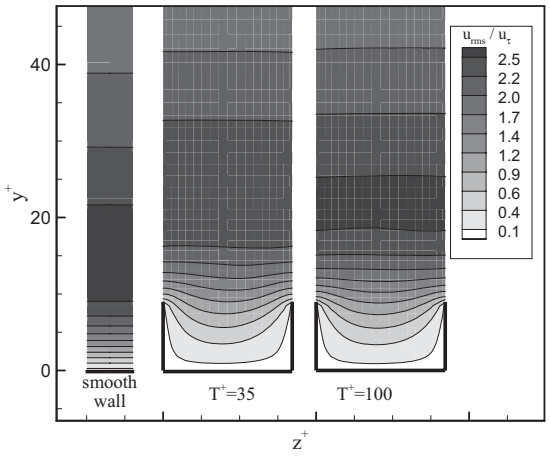

Figure 8: Contours of the streamwise velocity fluctuation based on phase-averaged data at $t^* = 0$.

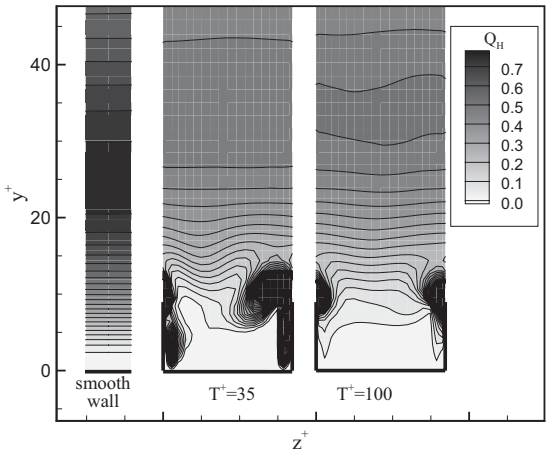

Figure 9: Contours of the phase-averaged Q_H at $t^* = 0$.

spanwise variation. Case B's maximum value is higher than the one of case A which seems to influence the vortical flow structures more effectively.

ANISOTROPY

Lumley and Newman (Lumley, 1977) presented the anisotropy invariant map which characterizes the state of turbulence with respect to its isotropy or - more commonly in wall-bounded flows - anisotropy. The map plots the second invariant II_a of the non-dimensional anisotropy tensor a_{ij} over its third invariant III_a.

$$a_{ij} = \frac{\overline{u_i' u_j'}}{2k} - \frac{1}{3}\delta_{ij} \tag{3}$$

$$II_a = a_{ij}a_{ji} \tag{4}$$

$$III_a = a_{ij}a_{jk}a_{ki} \tag{5}$$

The anisotropy tensor in equation 3 is constructed with the help of the turbulent kinetic energy k and the Kronecker symbol δ.

Figure 10 shows the anisotropy map along a wall-normal trajectory starting in the groove between two riblets. Both cases behave very similarly but nevertheless an important

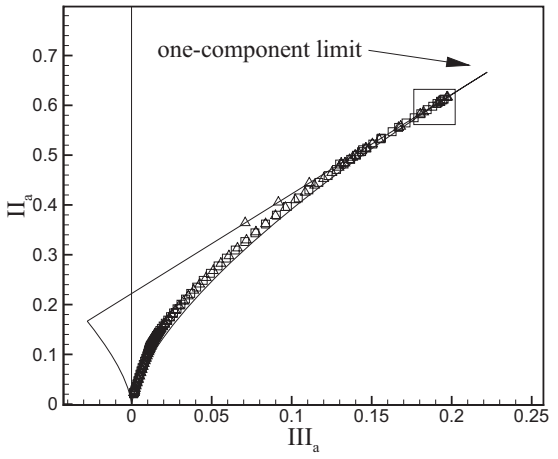

Figure 10: Anisotropy invariant map at phase angle 0° along the wall-normal midline between two riblets. △ $T^+ = 35$ (case A), □ $T^+ = 100$ (case B).

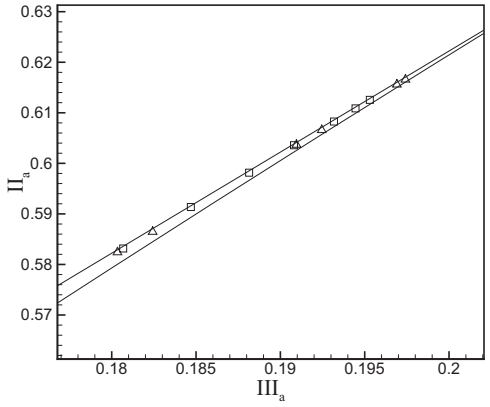

Figure 11: Anisotropy invariant map enlarged from the rectangle in figure 10. △ $T^+ = 35$ (case A), □ $T^+ = 100$ (case B).

difference can be observed. Case A approaches the one-component limit further than case B as the enlarged figure 11 demonstrates. It is characteristic of drag reducing methods that the more effective the method is the more the flow approaches the one component limit (Frohnapfel, 2007). Thus, the present cases are consistent with that characteristic behavior.

CONCLUSION

The overall drag reduction of riblets could be improved by oscillatory tilting riblets from 8.6% to 11.1%. The comparison between two oscillating cases has shown that the oscillation is more effective in terms of drag reduction when a strong secondary flow of low-speed fluid is present. The reason is that the low-speed fluid reduces the impact of high-speed fluid on the riblet tips in their most vulnerable phase when being in upright position.
Furthermore, it has been demonstrated that drag reducing cases with oscillation reduce turbulent fluctuation and vortical structures. These cases tend to a more anisotropic state of turbulence towards the one-component limit which agrees well with the characteristic behavior of various other drag reduction methods.

ACKNOWLEDGMENTS

This research was funded by the German Science Foundation (DFG) within the scope of the priority program Nature-Inspired Fluid Mechanics (SPP 1207). The simulations were performed on the National Supercomputer HLRB II (SGI Altix 4700) at the Leibniz-Rechenzentrum (LRZ), Munich, Germany.

REFERENCES

Baron, A. and Quadrio, M., "Turbulent drag reduction by spanwise wall oscillations," *Applied Scientific Research*, vol. 55, pp. 311-326, 1996.

Baron, A., Quadrio, A., and Vigevano, L., "On the boundary layer/riblets interaction mechanisms and the prediction of turbulent drag reduction," *Int. J. Heat and Fluid Flow*, vol. 14 (4), pp. 324-332, 1993.

Bechert, D.W. and Bartenwerfer, M., "The viscous flow on surfaces with longitudinal ribs," *J. Fluid Mech.*, vol. 206, pp. 105-129, 1989.

Bechert, D.W., Bruse, M., Hage, W., van der Hoeven, J.G.T., and Hoppe, G., "Experiments on drag-reducing surfaces and their optimization with an adjustable geometry," *J. Fluid Mech.*, vol. 338, pp. 59-87, 1997.

Choi, H., Moin, P., and Kim, J., "Direct numerical simulation of turbulent flow over riblets," *J. Fluid Mech*, vol. 255, pp. 503-539, 1993.

Choi, J.-I., Xu, C.-X., and Sung, J.S., "Turbulent Drag Reduction by Spanwise Wall Oscillation," *14th Australasian Fluid Mechanics Conference*, Adelaide, Australia, 2001.

Choi, K.S., DeBisschop, J.-R., and Clayton, B.R., "Turbulent boundary-layer control by means of spanwise-wall oscillations," *AIAA Journal*, vol. 36 (7), pp. 1157-1163, 1998.

Choi, K.S. and Clayton, B.R., "The mechanism of turbulent drag reduction with wall oscillation," *Int. J. Heat and Fluid Flow*, vol. 22, pp. 1-9, 2001.

Frohnapfel, B. and Lammers, P. and Jovanovic, J. and Durst, F., "Interpretation of the mechanism associated with turbulent drag reduction in terms of anisotropy invariants", *J. Fluid Mech.*, vol. 577, pp. 457-466, 2007.

Goldstein, D.B. and Tuan, T.-C., "Secondary flow induced by riblets," *J. Fluid Mech.*, vol. 363, pp. 115-151, 1998.

Jiménez, J. and Moin, P., "The minimal flow unit in near-wall turbulence," *J. Fluid Mech.*, vol. 225, pp. 213-240, 1991.

Jung, W.J., Mangiavacchi, N., and Akhavan, R., "Suppression of turbulence in wall-bounded flows by high-frequency spanwise oscillations," *Phys. Fluids A*, vol. 4 (8), pp. 1605-1607, 1992.

Karniadakis, G.E. and Choi, K.S., "Mechanisms on transverse motions in turbulent wall flows," *Annu. Rev. Fluid Mech.*, vol. 35, pp. 45-62, 2003.

Kim, J., Moin, P., and Moser, R., "Turbulence statistics in fully developed channel flow at low Reynolds number," *J. Fluid Mech.*, vol. 177, pp. 133-166, 1987.

Laadhari, F., Skandaji, L., and Morel, R., "Turbulence reduction in a boundary layer by a local spanwise oscillating surface," *Phys. Fluids*, vol. 6 (10), pp. 3218-3220, 1994.

Luchini, P., Manzo, F., and Pozzi, A., "Resistance of a grooved surface to parallel flow and cross-flow," *J. Fluid Mech.*, vol. 228, pp. 87-109, 1991.

Lumley, J. L. and Newman, G., "The return to isotropy of homogeneous turbulence", *J. Fluid Mech.*, vol. 82, pp. 161-178, 1977.

Miyake, Y., Tsujimoto, K., and Takahashi, M., "On the mechanism of drag reduction of near-wall turbulence by wall oscillation," *JSME Int. Journal, Series B*, vol. 40 (4), pp. 558-566, 1997.

Robinson, S.K., "Coherent motions in the turbulent boundary layer," *Annu. Rev. Fluid Mech.*, vol. 23, pp. 601-639, 1991.

Trujillo, S.M., Bogard, D.G., and Ball, K.S., "Turbulent boundary layer drag reduction using an oscillating wall," *AIAA Paper 97-1870*, 1997.

Walsh, M.J., "Riblets," *Prog. Astronaut. Aeronaut.*, vol. 123, pp. 203-261, 1990.

Wassen, E., et al., "Turbulent drag reduction by oscillating riblets," *AIAA 4th flow control conference*, AIAA-2008-3771, 2008.